13th International Symposium on Turbulence and Shear Flow Phenomena (TSFP13)
Montreal, Canada, June 25–28, 2024

ANALYSIS AND MODELING OF THE TIP LEAKAGE VORTEX OF AN AXIAL FAN USI7

Ahmadou Bamba DRAME, Marlène SANJOSE
Departement de génie mécanique
École de Technologie Supérieure
Montréal, Canada
ahmadou-bamba.drame.1@ens.etsmtl.ca

Natacha GALAND
École d'Ingénieurs SeaTech
Université de Toulon
Toulon, France

ABSTRACT

This numerical study focuses on modeling the tip leakage vortex (TLV) in a low-speed fan configuration named USI7. The Reynolds number based on the chord is 2.1×10^5 and the Mach number is 0.14, representative of flow in ventilation system. Two tip clearances are investigated corresponding to 0.4 and 4% of the tip chord. Incompressible simulations are carried out using the Reynolds-Averaged Navier-Stokes (RANS) method for several flow coefficients with ANSYS CFX and the $k-\omega$ SST turbulence closure model. The performance curve of the fan at design rotational speed obtained with the simulations are compared to the experimental measurements. In the following, the portion of losses associated with tip leakage flow are estimated in the simulation results using Denton approach for several flow coefficients. Then a loss model proposed recently by Deveaux for the tip leakage flow, based on a Rankine vortex model, is evaluated over different operational conditions for the low-speed $USI7$ fan.

INTRODUCTION

A clearance between the blade tip and the casing wall is necessary for the proper operation of a rotating machine. However, it can also be a major source of unfavorable flow phenomena, known as tip leakage flow (TLF), which is driven by the pressure rise generated the blade. Consequently, the TLF strengthens when the flow rate across the machine is reduced. Additionally, blade loading leads to the formation of a main vortex, known as the tip leakage vortex (TLV), similarly to the vortex formed at the edge of a finite span wing. At the gap exit, the TLF wraps around the TLV, which detaches from the blade. The vortical complex structures strongly interact with the main flow and decrease in strength (Liu *et al.*, 2019). The tip gap flow can cause significant performance losses in axial turbomachinery (Dixon & Hall, 2014). However, these mechanisms depend on several parameters such as: the tip gap size, the blade loading and the incoming casing boundary layer (Cumpsty, 1989). For predicting accurately the performances of a fan system at off-design operation, it is necessary to develop loss models that can capture the influence of tip leakage flow at various operating conditions.

The experimental configuration USI7 is noteworthy for method and model development. It corresponds to a generic low pressure rotor-only test fan installed in a constant cylindrical duct. This fan was designed by University of Siegen and has been intensively investigated both experimentally and numerically (Carolus *et al.*, 2015). In particular, fan performance and noise emission for two tip gap sizes have been investigated. The increase of tip gap from 0.4% to 4% of chord has been shown to yield 10% reduction in the total to static efficiency, and more than 10 dB noise increase at design operating condition (Carolus *et al.*, 2015). The configuration has been simulated with Reynolds-Averaged Navier-Stokes (RANS) method for several flow coefficients by Sanjosé & Pépin (2022). A mesh convergence study and turbulence model sensitivity analysis were performed. The results were evaluated against experimental results.

This study employs a RANS database of the USI7 configuration to assess a model for predicting the losses associated with tip gap flow. The final objective of this study is to verify and extend the recent model of Deveaux *et al.* (2020), which was developed for isolated airfoil and has been recently applied in a cascade configuration (Drame & Sanjose, 2023). Analyzing the RANS flow fields, the impact of varying the flow coefficient on the shape, path and strength of the TLV will be investigated and parametrized.

USI7 NUMERICAL DATABASE

The numerical configuration shown in Fig 1 mimics the USI7 fan installed in a long circular duct, as it has been experimentally tested at the University of Siegen (Carolus *et al.*, 2015), where the flow is sucked out of a large semi-anechoic room. The fan consists of 5 blades based on NACA 4-digit airfoil sections. The duct has a diameter of $D = 300$ mm. The blade chord varies from 86 mm at the hub to $c = 78$ mm at the tip. A constant tip clearance s is ensured between the blade tip and the duct inner wall. Two configurations will be considered,

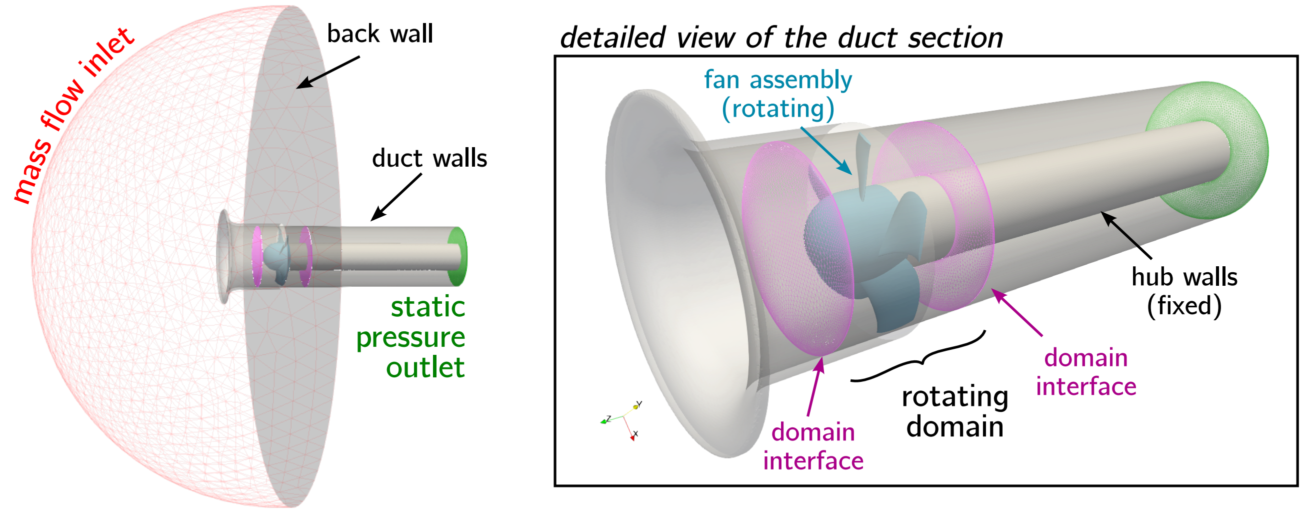

Figure 1. USI7 configuration: global and detailed parts.

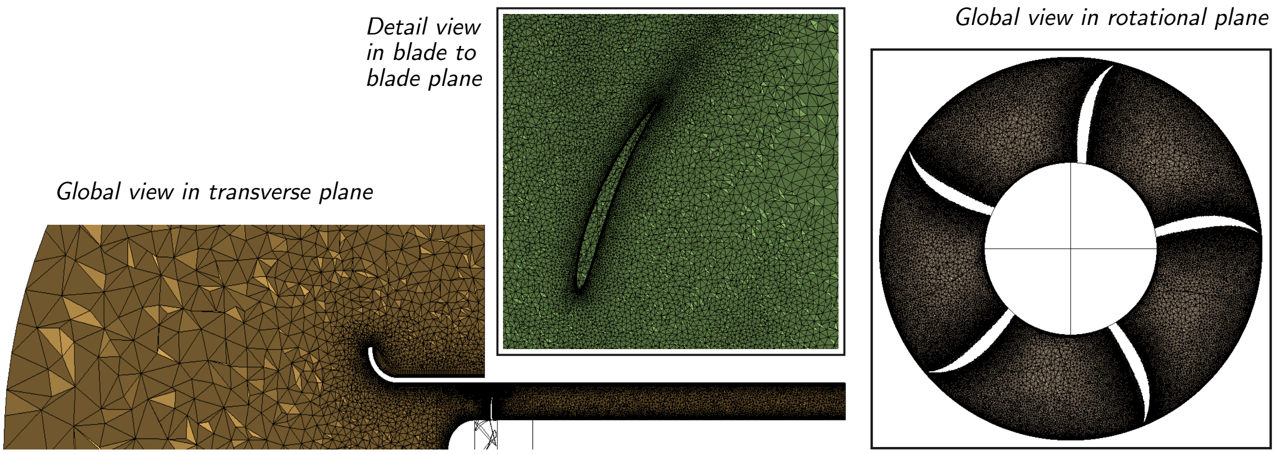

Figure 2. Visualizations of the mesh used in the present work.

one with a small clearance 0.3 mm and one with a large clearance $\tau = 3$ mm, which corresponds to about $\tau/c = 0.4\%$ and 4% of the blade chord at tip respectively. The simulations have been performed at the nominal rotation speed of $n = 3000$ rpm. The Reynolds number based on the blade chord and the entrainment velocity at tip is $Re = 2.2\times10^5$. The Mach number is $Ma = 0.14$, which justifies the incompressible approach adopted in the simulations. The steady-state simulations have been performed with the high resolution advection scheme of ANSYS CFX 2019.R4 incompressible solver using multiple reference frames. Thermal effects are neglected, and the air is modeled with a constant density $\rho = 1.16\ \mathrm{kg/m^3}$ and constant viscosity $\mu = 1.831\times10^{-5}\ \mathrm{kg/(m\cdot s)}$. The turbulence closure model $k-\omega$ shear-stress transport (SST) is used as it has been shown to be robust and relatively accurate to capture wall bounded flow at moderate Reynolds number (Menter *et al.*, 2003).

The computational domain is composed of 3 regions, the inlet and outlet regions are fixed in the absolute reference frame, while the rotor domain is rotating. No periodic conditions are defined as the three domains include the full 360° of the geometry. ANSYS CFX solver ensures the conservation of mass flux across the interfaces shown in pink in Fig 1. In the fixed domains, all the smooth walls are set with a no-slip boundary condition, except the back wall in contact with the hemisphere for simplicity. In the rotating domain the fan assembly (shown in blue in Fig 1) is set with a no-slip boundary condition in the local reference frame and the stationary hub part and the casing are set as counter-rotating wall in this domain. The characteristic curve of the fan is assessed by varying the mass flow rate $\dot{m}$ at the hemispheric inlet boundary condition (shown in red in Fig 1) while keeping the static outlet pressure to ambient atmospheric pressure with an allowance of 5 % deviation in average on that surface (shown in green in Fig 1). Several simulations are performed for flow coefficient φ swept between 0.14 and 0.2 where φ is defined by Eq. (1).

$$\varphi = \frac{\dot{m}}{\rho \frac{\pi^2}{4} D^3 n} \tag{1}$$

A mesh convergence study has been performed by Sanjosé & Pépin (2022). In the present work, the results obtained for the mesh designated V2 are used. The mesh is shown in Fig 2. It is composed of 77 million cells among which 30% are tetrahedrons and 70% prisms. The wall resolution wall units (y^+) is about 1 in average on the blade surface. This mesh is well refined near the tip gap, the duct walls and on the leading and the trailing edge.

PERFORMANCES

The performances of the USI7 fan are quantified in terms of pressure rise coefficient ψ and efficiency η given by Eqs. (2) and (3):

$$\psi = \frac{\Delta p_{ts}}{\rho \frac{\pi^2}{4} D^2 n^2} \tag{2}$$

$$\eta = \frac{\dot{m} \Delta p_{ts}}{\rho T n} \tag{3}$$

where Δp_{ts} is the total to static pressure rise between inlet and outlet surfaces and T the torque generated by the aerodynamic forces on the fan assembly. The comparison between the simulation database and the experiments (Carolus *et al.*, 2015) are given in Fig 3.

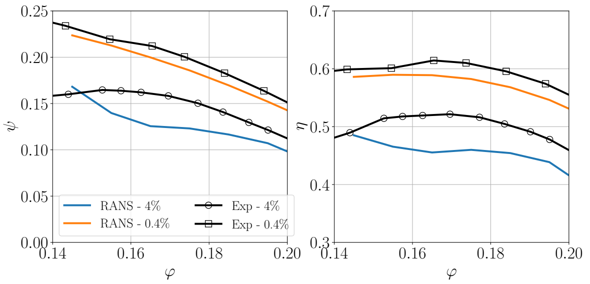

Figure 3. USI7 Performances.

As clearly seen in Fig. 3, the efficiency is reduced by 10% with the increased tip clearance. The discrepancies with experiments are considered to be caused by the limited accuracy of the employed RANS model for this configuration. In particular transitional flow and unsteady flow mechanisms have been shown to have important effects for the small and large clearance respectively (Sanjosé & Pépin, 2022; Zhu & Carolus, 2018).

LOSS ANALYSIS

In this section, the losses generated by the flow around the fan are evaluated. The losses are associated with the production of entropy in the machine (Denton, 1993). Given the adiabatic and incompressibility assumptions for the flow in the present low speed fan, only the viscous generation of entropy is evaluated in the RANS simulations using two approaches.

In the rotor reference frame, the entropy increase $\Delta s_{1\to 2}$ of the flow between an upstream plane 1 and downstream plane 2 can be computed from the decrease in the stagnation pressure P_t between these planes as demonstrated by Lakshminarayana *et al.* (1995). This first order approximation is given in Eq. (4), where R is the perfect gas constant, and P_t is the mass flow weighted relative total pressure (Cyrus, 1985).

$$\frac{\Delta s_{1\to 2}}{R} = \frac{P_{t,1} - P_{t,2}}{P_{t,1}} = \frac{(\Delta P_t)_{1\to 2}}{P_{t,1}} \tag{4}$$

The loss coefficient ζ is defined by Eq. (5) as the ratio of the stagnation pressure loss $(\Delta P_t)_{1\to 2}$ and the inlet reference dynamic pressure (Lakshminarayana *et al.*, 1995).

$$\zeta = \frac{(\Delta P_t)_{1\to 2}}{P_{t,1} - P_{s,1}} \tag{5}$$

Another approach to evaluate the losses is by the local entropy generation rate. The entropy generation caused by the turbulent kinetic energy is computed from the eddy viscosity μ_t resolved by the RANS model (Fiore *et al.*, 2021).

$$\dot{s} = \frac{1}{T} (\mu + \mu_t) \left(\frac{\partial U_i}{\partial x_j} + \frac{\partial U_j}{\partial x_i} \right) \frac{\partial U_i}{\partial x_j} \tag{6}$$

The loss coefficient ζ is then defined by Eq. (7) from the integration of the entropy generation rate over the entire volume between planes 1 and 2.

$$\zeta = \frac{\rho T \iiint_{\mathscr{V}} \dot{s} dv}{\dot{m} \left(P_{t,1} - P_{s,1} \right)} \tag{7}$$

The integration volume $\mathscr{V}$ in Eq. (7) can be restricted to identify the contribution of specific flow features. In the present work, the contribution of the boundary layer on the blades is computed by selecting a volume of 2.5 mm around the blades. The tip gap-flow contribution is obtained by integrating over the external 20% portion of the duct section in the rotor domain, but excluding the blade, casing and hub 2.5 mm proximity.

Figure 4 shows the losses as a function of the flow coefficient for the two gap clearances for the volume between planes 1 and 2 defined at 10 cm upstream and downstream from the rotor blades. On the left, the coefficient ζ evaluated with the two approaches, namely the "P_t flux" approach from Eq. (5) and the "$\dot{s}$ volume" approach from Eq. (7). First it can be clearly seen that a major difference of about 5% exists between the two gap configurations. Also, the losses increase as the flow coefficient is reduced. The two approaches to evaluate the losses show similar trends, but important differences can be identified. The "$\dot{s}$ volume" is prompt to larger inaccuracies due to the discrete volume integration operated in the present work (Fiore *et al.*, 2021). For that reason, this approach will be limited here to evaluate the loss contributions of the tip-gap flow as a function of the flow coefficient. The contribution for the tip flow and the profile (boundary layers developing on the blades) are shown in percentage of the total computed entropy increase between plane 1 and 2 in Fig. 4 right. While in the small clearance case, the profile losses are the primary ones, the tip gap flow associated losses are the dominant ones in the large clearance case. For both clearance ratio, the profile losses are increasing with the flow rate, while the tip gap flow contribution has an opposite trend.

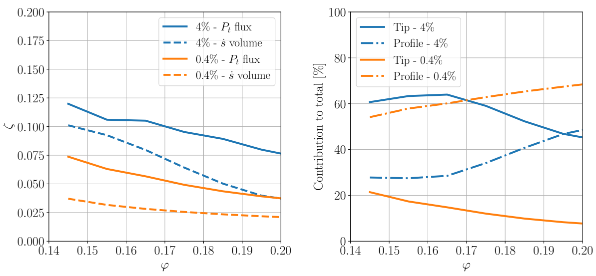

Figure 4. Viscous loss analysis for the two clearances.

In the following, the losses associated with the tip gap flow for the two configurations are obtained from the contribution of the tip gap flow shown on the right in Fig. 4 and the total viscous loss obtained with the "P_t flux" approach displayed with continuous lines on the left in Fig. 4.

The model for losses associated with the tip gap flow proposed by Deveaux *et al.* (2020) has been developed based on observation and quantification obtained from advanced experimental flow analysis of an isolated airfoil with a gap configuration. In the present work, the main assumptions of the model will be investigated for the present USI7 low speed flow configuration using the RANS database.

TIP LEAKAGE VORTEX

The main assumption made by Deveaux *et al.* (2020) is that the tip gap flow losses ζ_t are proportional to the square of the tip leakage vortex strength Γ. In the present work, all quantities are extracted in the rotating reference frame attached to the fan blades. The vortex strength is computed in a plane perpendicular to the blade mean camber line at tip. The vortex strength can be recast as the vorticity flux through a surface $\mathscr{S}_t$ delimiting the vortex :

$$\Gamma = \oint \vec{V} \cdot \vec{dl} = \iint_{\mathscr{S}_t} \vec{\omega} \cdot \vec{dS} = \iint_{\mathscr{S}_t} \omega_n \, dS \qquad (8)$$

where $\vec{\omega} = \nabla \times \vec{V}$ is the vorticity and ω_n the vorticity component parallel to the blade. In this work, the surface $\mathscr{S}_t$ corresponds to the area of the normal plane at 70% of the chord for which $Q > 2 \times 10^5\,\mathrm{s}^{-2}$. The Q criterion corresponds to the second invariant of the velocity gradient tensor (Hunt *et al.*, 1988). In addition, to exclude induced vortices that are counter rotating, the zone is also limited by a criterion on $\omega_n > 0$. Additional thresholds on distance from the blade suction side are defined to restrict $\mathscr{S}_t$ to the primary tip leakage vortex and exclude boundary layer zones. The center of the vortex is then determined as the minimum pressure on this surface Chakraborty *et al.* (2005). Finally, the vortex strength is made dimensionless by the chord at tip and a reference velocity W_∞. For consistency with the loss coefficient definition, the latter is defined by the mass flow averaged over the duct section of the relative dynamic pressure.

$$W_\infty = \sqrt{\frac{2}{\rho}\left(P_{t,1} - P_{s,1}\right)} \qquad (9)$$

The comparison between the estimated tip gap losses and the scaled vortex strength is provided in Fig. 5 for different flow coefficient. While the vortex strength evolves as a function of the flow coefficient for the large clearance case, it remains almost constant for the small clearance configuration. This effect is thought to be related to inaccuracies in both the vortex detection and the vorticity surface integral. Indeed, in this configuration with clearance of 0.4% tip chord, the tip leakage vortex is very coherent, small and very close from the casing where it interacts with the end wall boundary layer. For the larger tip gap of 4% tip chord, the trend is very well captured for the high flow coefficients above the maximum pressure rise point at $\varphi = 0.165$. For lower flow coefficients, the tip vortex structure is more complex as the tip leakage vortex experience a breakdown that enhances the losses. This is not captured with the present vortex strength computation as induced and separation vortex are not accounted for.

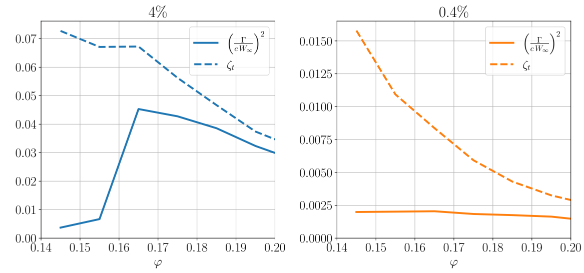

Figure 5. Comparison of tip leakage vortex strength (continuous line) and associated losses (dashed line) for large clearance (left) and small clearance (right).

TIP LEAKAGE THROUGH THE GAP

The second assumption made by Deveaux *et al.* (2020) is that the strength of the tip leakage vortex is related to the momentum of the leakage jet flow through the gap which in turns is driven by the pressure jump across the gap. The tip leakage vortex and its image with respect to the casing form a horseshoe vortex sheet whose lift is related to the thrust of the tip leakage jet. This assumption is recast into Eq. (10) as the dimensionless tip leakage vortex strength Γ being proportional to $\chi_D^2 C_L$ where χ_D is the discharge coefficient caused by the *vena contracta* at entrance of the tip gap, and C_L is the lift coefficient of the airfoil. The proportionality coefficient is given by the ratio $\tau/\Delta r_t$ of the tip gap clearance to the vortex sheet half-span, which corresponds to the vortex distance from the casing.

$$\frac{\Gamma}{cW_\infty} = \frac{\tau}{\Delta r_t} \chi_D^2 C_L \qquad (10)$$

In the present evaluation, the airfoil lift coefficient is replaced by the blade lift coefficient, which is obtained by summing of the lift coefficients of 10 blade segments. For each segment, the lift is defined as the aerodynamic force component perpendicular to the local relative flow velocity. The discharge coefficient is estimated using Eq. (11) from the potential flow theory of Moore & Tilton (1988), for which it is related to σ, the contraction coefficient of the jet flow within the tip gap.

$$\chi_D = \sigma / \sqrt{1 - 2\left(\sigma - \sigma^2\right)} \qquad (11)$$

To compute σ, the leakage flow is analyzed over the entire tip edge. The distribution of the mass flow rate per unit length $\dot{m}_j(\xi)$ is computed perpendicular to the mean camber line of the tip edge profile. In addition, the profiles of the velocity component perpendicular to the mean camber line are extracted in the gap. From these profiles, the maximum velocity $U_{\max}(\xi)$ is obtained along the mean camber line. From these quantities, the local contraction coefficient is obtained as shown in Eq. (12). In addition, the total leakage flow rate can be computed by integration over the mean camber line and a uniformity factor $\Theta(\xi)$ can be computed.

$$\sigma(\xi) = \frac{\dot{m}_j(\xi)}{\rho\,\tau U_{\max}(\xi)} \tag{12}$$

$$\overline{\dot{m}_j} = \frac{1}{c}\int_0^c \dot{m}_j(\xi)d\xi \tag{13}$$

$$\Theta(\xi) = 1 + \frac{\dot{m}_j(\xi) - \overline{\dot{m}_j}}{\overline{\dot{m}_j}} \tag{14}$$

The uniformity and local contraction factors are shown in Fig. 6. The configuration with the largest tip clearance demonstrates the highest non-uniformity with Θ values largely different from 1. The peak in uniformity factor identifies the location of the maximum of leakage over the tip edge. For low flow coefficient, the maximum is near the leading edge around 15% chord, while at high flow coefficient the maximum is located above 50%. While for the low tip gap, the contraction factor is almost constant around 0.80 for all flow coefficients, the contraction factor varies from 0.70 to 0.85 depending on flow coefficient.

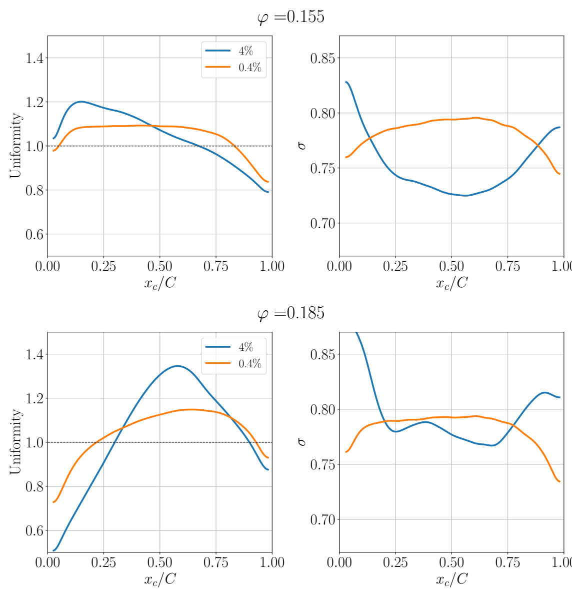

Figure 6. Uniformity and contraction factors for two flow conditions.

The integrated mass flow rate $\dot{m}_j = c\overline{\dot{m}_j}$ is compared for the two gap configurations in Fig. 7 as a function of the flow coefficient. With the large tip clearance, the leakage flow rate is about 10 times larger than for the smallest tip clearance. Still the leakage remains small, up to 1.2% of the main flow rate across the fan. The maximum leakage is shifted by about 10% of the chord towards the trailing edge with the small tip clearance. At low flow coefficient, the maximum leakage moves to the front of the blade, exposing the blade to stall (Vo, 2010).

For the evaluation of the expression Eq. (10) between vortex strength and leakage jet flow momentum, the discharge coefficient χ_D is evaluated using Eq. (11) with σ extracted at the maximum leakage location displayed in Fig. 7 (right). The distance Δr_t is measured between the casing and the centroid of the vortex surface $\mathscr{S}_t$ used for the vortex strength calculation. Figure 8 shows the comparison of the evaluation obtained

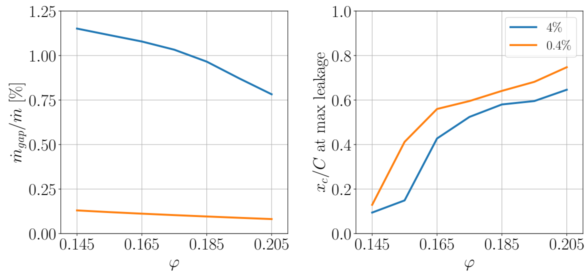

Figure 7. Tip leakage mass flow rate and location of maximum leakage as function of flow coefficient.

for the left and right terms in Eq. (10) for the two configuration as a function of flow coefficient. For both configurations, the trends obtained by the two separate estimations is well captured. However, the two evaluations are not equals, and the vortex strength appears 3 to 4 times smaller than the right-hand term associated to the leakage. These discrepancies might be caused by the vortex strength evaluation itself, as the proper definition of the integration surface $\mathscr{S}_t$ is not straightforward. In addition, Eq. (10) can be seen as the conversion of the blade lift into a tip edge vortex as for an isolated wing of finite span. But in the case of tip gap flow, the vortex structure is more complex and the induced and separation vortices, not accounted for in the present work, may also collect a portion of the total strength.

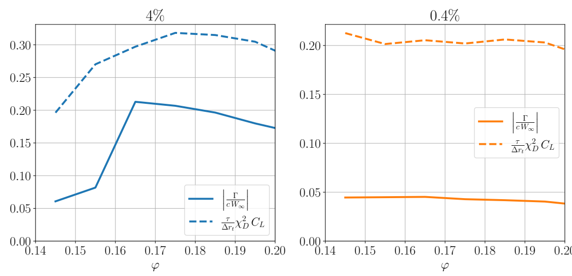

Figure 8. Evaluation of Eq. (10) between vortex strength and leakage jet flow momentum.

EVALUATION OF LOSS MODEL

Using Eq. (10) squared, Deveaux *et al.* (2020) provides a model of tip gap losses that can be of interest for design. Using the viscous loss evaluation and the tip leakage jet flow analysis from the last two section, the left and right terms of Eq. (15) are compared in Fig. 15. The same limited accuracy as in Fig. 7 is obtained.

$$\zeta_t = \left(\frac{\tau}{\Delta r_t}\right)^2 \chi_D^4 C_L^2 \tag{15}$$

CONCLUSIONS

The present work focus on the evaluation of the model recently proposed by Deveaux *et al.* (2020) for the estimation of losses associated with the tip gap flow. The initial model was developed for an isolated airfoil with gap. In the present work, the different assumptions and quantities that appear in the model are evaluated using a large RANS database of a low-speed fan installed in a circular duct. While the model and the different quantities appear to provide good trends, the model can not provide accurate loss evaluations. The model could be improved by accounting for the strength of secondary vortices present in the complex tip gap flow. In addition, using larger fan database may help in providing more accurate calibration for such models.

REFERENCES

Carolus, T., Zhu, T. & Sturm, M. 2015 A low pressure axial fan for benchmarking prediction methods for aerodynamic performance and sound. *Noise Control Engineering Journal* **63** (6), 537–545.

Chakraborty, Pinaki, Balachandar, S. & Adrian, Ronald J. 2005 On the relationships between local vortex identification schemes. *Journal of Fluid Mechanics* **535**, 189–214.

Cumpsty, N. A. 1989 *Compressor Aerodynamics*. Harlow, Essex, England : New York: Longman Scientific & Technical ; J. Wiley.

Cyrus, Václav 1985 Experimental investigation of losses and secondary flow in an axial compressor stage. *Forschung im Ingenieurwesen A* **51** (2), 33–40.

Denton, J. D. 1993 The 1993 IGTI Scholar Lecture: Loss Mechanisms in Turbomachines. *Journal of Turbomachinery* **115** (4), 621–656.

Deveaux, B., Fournis, C., Brion, V., Marty, J. & Dazin, A. 2020 Experimental analysis and modeling of the losses in the tip leakage flow of an isolated, non-rotating blade setup. *Experiments in Fluids* **61** (5), 126.

Dixon, S. L. & Hall, C. A. 2014 *Fluid Mechanics and Thermodynamics of Turbomachinery*, seventh edition edn. Amsterdam ; Boston: Butterworth-Heinemann is an imprint of Elsevier.

Drame, A.B & Sanjose, M 2023 Analyse, classification et modélisation des pertes dans une grille rectiligne de compresseur avec jeu. In *Computational Fluid Dynamics Canada International Congress*, p. 6. Sherbrooke, Canada.

Fiore, M., Daroukh, M. & Montagnac, M. 2021 Loss assessment of a counter rotating open rotor using URANS/LES with phase-lagged assumption (draft). *Computers & Fluids* **228**, 105025.

Hunt, J., Wray, Alan & Moin, Parviz 1988 Eddies, streams, and convergence zones in turbulent flows. *Studying Turbulence Using Numerical Simulation Databases* pp. 193–208.

Lakshminarayana, B., Zaccaria, M. & Marathe, B. 1995 The Structure of Tip Clearance Flow in Axial Flow Compressors. *Journal of Turbomachinery* **117** (3), 336–347.

Liu, Yangwei, Zhong, Luyang & Lu, Lipeng 2019 Comparison of DDES and URANS for Unsteady Tip Leakage Flow in an Axial Compressor Rotor. *Journal of Fluids Engineering* **141** (121405).

Menter, F R, Kuntz, M & Langtry, R 2003 Ten Years of Industrial Experience with the SST Turbulence Model. In *4th International Symposium on Turbulence, Heat and Mass Transfer*, pp. 625–632. West Redding.

Moore, J. & Tilton, J. S. 1988 Tip Leakage Flow in a Linear Turbine Cascade. *Journal of Turbomachinery* **110** (1), 18–26.

Sanjosé, M & Pépin, P 2022 Aeroacoustic analysis of an axial fan. In *International Conference on Fan Noise, Aerodynamics, Applications and Systems*. Senlis, France.

Vo, Huu D. 2010 Role of Tip Clearance Flow in Rotating Instabilities and Nonsynchronous Vibrations. *Journal of Propulsion and Power* **26** (3), 556–561.

Zhu, T & Carolus, Thomas H 2018 Axial fan tip clearance noise: Experiments, Lattice–Boltzmann simulation, and mitigation measures. *International Journal of Aeroacoustics* **17** (1-2), 159–183.